



HAL
open science

Is the local seismicity in western Hispaniola (Haiti) capable of imaging northern Caribbean subduction?

J. Corbeau, O.L. Gonzalez, V. Clouard, F. Rolandone, S. Leroy, D. Keir, G. Stuart, R. Momplaisir, D. Boisson, C. Prépetit

► To cite this version:

J. Corbeau, O.L. Gonzalez, V. Clouard, F. Rolandone, S. Leroy, et al.. Is the local seismicity in western Hispaniola (Haiti) capable of imaging northern Caribbean subduction?. *Geosphere*, 2019, 10.1130/GES02083.1 . hal-02325330

HAL Id: hal-02325330

<https://hal.science/hal-02325330v1>

Submitted on 25 Nov 2020

HAL is a multi-disciplinary open access archive for the deposit and dissemination of scientific research documents, whether they are published or not. The documents may come from teaching and research institutions in France or abroad, or from public or private research centers.

L'archive ouverte pluridisciplinaire **HAL**, est destinée au dépôt et à la diffusion de documents scientifiques de niveau recherche, publiés ou non, émanant des établissements d'enseignement et de recherche français ou étrangers, des laboratoires publics ou privés.

Is the local seismicity in western Hispaniola (Haiti) capable of imaging northern Caribbean subduction?

Corbeau J.^{1,2}, Gonzalez O.L.³, Clouard V.^{1,2}, Rolandone F.⁴, Leroy S.⁴, Keir D.^{5,6},
Stuart G.⁷, Momplaisir R.⁸, Boisson D.⁸, and Prépetit C.⁹

¹ Université de Paris, Institut de Physique du Globe de Paris, CNRS, UMR 7154, F-97250 Saint-Pierre, France.

² Observatoire Volcanologique et Sismologique de Martinique, Institut de Physique du Globe de Paris, CNRS, F-97250 Saint-Pierre, France.
corbeau@ipgp.fr; clouard@ipgp.fr

³ Centro Nacional de Investigaciones Sismológicas (CENAIIS), Ministerio de Ciencia, Tecnología y Medio Ambiente, Cuba.
oleary@cenais.cu

⁴ Sorbonne Université, CNRS-INSU, Institut des Sciences de la Terre Paris (ISTeP), Paris, France.
frederique.rolandone@sorbonne-universite.fr; sylvie.leroy@sorbonne-universite.fr

⁵ Ocean and Earth Science, National Oceanography Centre, University of Southampton, European Way, Southampton, U.K.

⁶ Dipartimento di Scienze della Terra, Università degli Studi di Firenze, Florence, Italy.
D.Keir@soton.ac.uk

⁷ School of Earth and Environment, University of Leeds, Leeds, UK.
G.W.Stuart@leeds.ac.uk

⁸ Université d'Etat d'Haiti, Faculté des Sciences, Port-au-Prince, Haiti.
roberte.momplaisir@laposte.net; dmboisson@yahoo.com

⁹ Unité Technique de Sismologie, Bureau des Mines et de L'Energie, Port-au-Prince, Haiti.
claudeprepetit@hotmail.com

1 **Abstract**

2 The boundary between the Caribbean and North American plates in the
3 Hispaniola region is the northwestern termination of the North American plate
4 subduction evolving from westward subduction in the Lesser Antilles to
5 southward subduction in the Greater Antilles, and oblique collision against the
6 Bahamas platform in Cuba. We analyze P-waveforms recorded by 27 broadband
7 seismic temporary stations deployed during the Trans-Haiti project. Seismicity
8 recorded by the temporary network from June 2013 to June 2014 is used to locate
9 the earthquakes. A total of 514 events were identified with magnitudes ranging
10 from 1 to 4.5. 26 moment tensors were calculated by full waveform inversion
11 using the ISOLA software. The analysis of the new moment tensors for the Haiti
12 upper lithosphere indicates that normal, thrust and strike-slip faulting are present
13 but with a majority of thrust faulting. The mean P- and T-axes for the moment
14 tensors indicated that the current compressional deformation is mainly N-S to
15 NNE-SSW. Moreover, a dozen intermediate-depth earthquakes (> 70 km) are
16 located under Haiti, with one event in the south of the island reaching 260 km
17 depth. The seismic data of the Haiti network, over a one-year time period, tend to
18 confirm the existence of a lithospheric slab inherited from southward subduction
19 under the Greater Antilles. The scarcity of the intermediate-depth seismic events
20 in this area may be the effect of the lack of a dense seismic network or may indicate
21 that we image the western slab edge.

22

23 **1. Introduction**

24 Recently, the Mw 7.0 2010 Haiti transpressional earthquake prompted
25 several geological and geophysical studies to constrain the fault geometry and the

26 crustal structure in the area of the mainshock near the capital city Port-au-Prince
27 (Calais et al., 2010; Mercier de Lépinay et al., 2011; Douilly et al., 2013; Leroy et
28 al., 2015). However, as sadly reminded by the October 7th, 2018 Mw 5.9 and Mw
29 5.4 earthquakes occurring in the north of Haiti, our knowledge of the local
30 seismicity remains very limited in the absence of a dense permanent seismic
31 network in Haiti. Many questions remain unresolved, as for example where the
32 current deformation is accommodated at the surface and at depth, and if there is
33 a subducting slab or a remnant slab under Haiti.

34 The Trans-Haiti project, a temporary seismic network consisting of 27
35 stations was deployed in Haiti from April 2013 for nearly 14 months to record the
36 local seismicity. One year of local events have been located and associated focal
37 mechanisms have been computed. In addition, we analyzed seismograms from 3
38 permanent stations in Haiti and from Cuba, Jamaica, Dominican Republic and
39 Bahamas to improve the network coverage in this period of time. The precise
40 knowledge of seismic source parameters (such as earthquake location, and fault-
41 plane solution) is a key for understanding physical processes on faults during
42 earthquakes and regional deformation style.

43 This paper focuses on the local seismicity using the Trans-Haiti temporary
44 network of 27 seismometers cross-cutting Haiti. The aim of this study is to
45 determine where the most active faults are located, and the current type of
46 faulting based on focal mechanisms. We use the local seismicity to improve the
47 knowledge of the crustal structure of Haiti and to constrain what happens deeper
48 in the lithosphere.

49

50 **2. Structural setting and previous studies**

51 Haiti, the western part of Hispaniola Island, is located at the boundary
52 between the North American plate and the Caribbean plate (Fig. 1). Haiti is a part
53 of the Cretaceous volcanic island arc formed at the boundary of the Pacific realm
54 called the Greater Antilles arc (Burke, 1988; Pindell et al., 2006). The Greater
55 Antilles arc now consists of part of Cuba, Hispaniola and Puerto Rico islands (Mann
56 et al., 1995). It constitutes two thirds of Hispaniola Island, and is mainly made up
57 of arc magmatic facies (Boisson, 1987; Escuder-Viruete et al., 2006). The Greater
58 Antilles arc became an inactive intra-oceanic arc at the end of the Late Cretaceous
59 when it collided with the Bahamas carbonate platform (Leroy et al., 2000; Cruz-
60 Orosa et al., 2012; Iturralde-Vinent, 2006).

61 Currently, the boundary between Hispaniola and the North American plate
62 is the northwestern termination of the Lesser Antilles subduction zone, as the
63 west dipping subduction under the Lesser Antilles transitions into a south dipping
64 subduction beneath Hispaniola and Puerto-Rico (McCann and Sykes, 1984).
65 However, this south dipping subduction is interpreted to end in the middle of
66 Hispaniola, a hypothesis based on the absence of deep seismicity (Symithe et al.,
67 2015). Therefore, the plate boundary in western Hispaniola is interpreted to
68 instead be an oblique collision.

69 The oblique motion of the Caribbean plate occurs at about 20 mm/yr
70 toward the NE relative to the North American plate (Calais et al., 2002). The
71 transpressional deformation is partitioned between several strike-slip and
72 thrusting structures. In Haiti, the main structures are (from N to S) the North
73 Haitian thrust fault, the sinistral strike-slip Septentrional-Oriente fault zone, the
74 Trans-Haitian fold and thrust belt, and the sinistral strike-slip Enriquillo-Plantain-
75 Garden fault zone (Fig. 1). A block modeling study based on GPS data shows that

76 the movement is currently transpressional on the Enriquillo-Plantain-Garden
77 fault zone, with a major compressional component, while it is mainly strike-slip
78 on the Septentrional-Oriente fault zone (Benford et al., 2012). Another study with
79 an improved data set (Symithe et al., 2016) shows that the active strain
80 accumulation in the southern part of the island involves an additional significant
81 component of N-S shortening. A seismic reflection study indicates that several
82 active thrusts are present offshore in the Gulf of Gonâve (Corbeau et al., 2016). A
83 receiver function study finds that the depth of the Moho across Haiti is variable,
84 ranging from 16 to 45 km, and that three distinct crustal terranes are accreted
85 along the plate boundary (Corbeau et al., 2017).

86

87 **3. Data and method**

88 **3.1 Data**

89 Data come from the Trans-Haiti temporary network that was deployed in
90 Haiti in April 2013 and recorded until June 2014 (Fig. 2). We installed 27
91 broadband stations (11 CMG-6TD and 16 CMG-40 TD), mainly along a north-south
92 profile to image the crustal structure of western Hispaniola (Corbeau et al., 2017).
93 A number of stations are also geographically distributed and complement the 5
94 permanent broadband stations from the Bureau des Mines et de l'Energie (BME)
95 and the Natural Resources of Canada (NRCAN) to characterize the local seismicity.
96 When data are available, we also add the records of stations from Dominican
97 Republic, Cuba, Bahamas, and Jamaica (Fig. 2) to improve the event locations and
98 the focal mechanism inversions.

99

100 **3.2 Location of seismic events**

101 We use the SeisComp3 software for our events database (Hanka et al.,
102 2010). To automatically detect the seismic events on the stations records, we use
103 a new application, Seismic Data Playback code (SDP), developed at the OVSM-IPGP
104 (Observatoire Volcanologique et Sismologique de Martinique, Institut de Physique
105 du Globe de Paris) (SDP is available on GitHub, [https://github.com/ovsm-](https://github.com/ovsm-dev/sdp)
106 [dev/sdp](https://github.com/ovsm-dev/sdp)). One has to note that the SDP interface is still under development and
107 this is the first time that it has been used on real data (Supplemental File 1). SDP
108 is a semi-automatic interface for the post-campaign seismic data processing. It
109 enables fast reading of the data and the automatic extraction of potential seismic
110 events that are detected with a STA/LTA (Short Time Average/Long Time
111 Average) filter. It generates Python ObsPy code for the offline analysis of seismic
112 data (Beyreuther et al., 2010). When two distinct pulses are identified (P and S
113 waves) on at least three stations, a seismic event is considered on the related
114 portion of the seismogram. Trans-Haiti data are relatively noisy and the specific
115 north-south distribution of the seismic stations result in a high dependency of the
116 triggering events on the choice of the STA/LTA parameters. Typically, we ran SDP
117 with the set of STA/LTA parameters of 2.8s and 22.5s respectively (Supplemental
118 File 1). Triggered events are then visually validated and sent to the SeisComp3
119 interface scolv. The P and S phases are then manually picked and earthquake
120 locations are computed with HYPO71 (Lee and Lahr, 1972), NonLinLoc (Lomax et
121 al., 2000) and LOCSAT. The locations are accepted when the root mean square
122 travel time residual (RMS) is < 0.35 . Crustal velocity models exist for Haiti but only
123 for the southern part of the island (Douilly et al., 2013). However, Corbeau et al.
124 (2017) show that the Moho depth and the crustal composition are highly variable
125 across Haiti. A velocity model applicable only for the southern part could not be

126 used for the whole island, and we use a crustal velocity model adapted from the
127 one of Dorel (1978) that is used in the Lesser Antilles. This 1D model consists of
128 three crustal layers with 3, 15 and 30 km of thicknesses and V_p (P velocities) of
129 3.5, 6.0 and 7.0 km/s. The mantle is then represented by a half space with a P
130 velocity of 8.0 km/s, and the V_p/V_s ratio is 1.76 for all the layers. Finally, we
131 compute the duration magnitude for $M < 3.5$ and the local magnitude on the vertical
132 components, M_{lv} for $M > 3.5$.

133

134 **3.3 Focal mechanisms calculations**

135 To compute focal mechanisms by full waveform inversion we use the
136 software package ISOLA-GUI (Sokos and Zahradnik, 2008). The methodology is
137 based on the iterative deconvolution technique, adjusted for regional and local
138 distances. Prior to the inversion process, we inspect all the data to choose only the
139 events where P and S waves are well identified. We use ISOLA to pre-process the
140 data (integration, instrument correction, origin alignment, signal to noise ratio).
141 Stations with inconsistent results are removed from the data set. For the
142 waveform inversion, we use the same velocity model as for the location of the
143 seismic events (see section 3.2). Density values are from Nafe and Drake (1960)
144 and attenuation quality factors Q_p and Q_s are from Graves and Pitarka (2010),
145 with $Q_s = 50 V_s$ and $Q_p = 2 Q_s$.

146 The moment tensors are calculated during the full waveform inversion by
147 a least squares method. In addition, centroid position and time are also calculated
148 by grid searching. We first performed a spatial grid search vertically on trial
149 sources around the hypocenter (step of 1 km) and in an interval of ± 3 s around
150 the origin time (step of 0.09 s). This gives us an approximation of the source depth

151 (Fig. 3a). Then a second grid search is performed on a plane around the depth
152 preferred in the first grid search, with steps of 1 km. The inversion frequencies are
153 chosen as a function of the hypocentral distances and the magnitudes of the events
154 (Sokos and Zahradnik, 2013).

155 Several parameters are plotted after the inversion to estimate the
156 robustness of the solution. We first plot the synthetic waveforms, generated for
157 the calculated moment tensor solution, versus the observed waveform from the
158 real seismogram (Fig. 3b). The Kagan angle describes in one single value the
159 deviation of a given solution from the reference solution (deviations of strike, dip,
160 and rake). The Kagan angle value of lower than 15 represents good stability of the
161 solution (Zahradnik and Custodio, 2012). In addition, the Condition Number (CN)
162 is useful in judging how well the inverse problem is posed, large $CN > 10$ indicating
163 an unstable solution (Krizova et al., 2013). We selected only the inversions for
164 which at least 9 components are used and with a signal to noise ratio of a minimum
165 of 2. Finally, Variance Reduction (VR) and Double-Couple percentage (DC) also
166 characterize the best-fitting solution. These values should both be as high as
167 possible, and always $> 30\%$.

168

169 **3.4 Calibration**

170 In order to check the validity of the velocity model and the inversion
171 parameters, we relocate a TNT shot and a Mw 5.8 earthquake identified by the
172 global catalogs (USGS and GCMT). The Mw 5.8 earthquake occurred the
173 05/28/2014 in the Mona Passage between Hispaniola and Puerto Rico. The
174 different locations and the associated focal mechanisms from GCMT, USGS and our
175 study are indicated in Table 1. The GCMT and USGS epicenters are separated by

176 39 km and the hypocenters are at depths of 89 km and 100.5 km respectively. By
177 comparison, the epicenter calculated in our study is 46 km from the GCMT
178 solution, and our hypocenter is 16 km deeper (105 km versus 89 km for the GCMT
179 solution). Our epicenter is also 44 km away from the USGS epicenter and our
180 hypocenter is 4.5 km deeper. Although the locations differ, they are in the same
181 range of variability. The magnitudes are the same (M_w 5.8) and the three moment
182 tensors are similar (maximum 13° , 8° and 12° of variability in the strike, dip and
183 rake respectively), validating our choice of inversion parameters used for the focal
184 mechanism. The TNT shot was made the 11/28/2013 in Dominican Republic, the
185 eastern part of Hispaniola Island, near the Haitian border. From our seismic data,
186 we locate this event at 3 km from its actual location, and only 400m deeper (Table
187 1). The RMS of our location is 0.03 with horizontal and vertical error bars of 1 km
188 and 3 km respectively, which indicates that the velocity model we use is sensible.
189 We conclude that our locations and inversion parameters retrieve robust moment
190 tensors.

191

192 **4. Results**

193 **4.1 Local Seismicity**

194 From June 2013 to June 2014, we have located 514 seismic events in Haiti
195 with magnitudes ranging from 1 to 4.5 (Fig. 4). These earthquakes are
196 predominantly shallow (<20 km), and several clusters can be identified in the
197 south of the study area. Two clusters are located at the eastern and western
198 extremities of a fault model proposed by Mercier de Lépinay et al. (2011) for the
199 2010 M_w 7.0 earthquake, aligned along the Enriquillo-Plantain-Garden fault zone
200 surface trace. A cluster of small magnitude events exists in the extreme south of

201 Haiti, near the border with the Dominican Republic, in an area shifted to the south
202 of Enriquillo-Plantain-Garden fault zone. Just behind the Haitian border, in
203 Dominican Republic, a cluster of seismic events is identified along the northern
204 side of the Enriquillo Lake (enlargement in Fig. 4): in June and July 2013, 51
205 earthquakes occurred with magnitudes ranging from 2.3 to 3.8 and depths ranging
206 from 1 km to 33 km. To the north, small seismic clusters are present at the eastern
207 end of the Septentrional-Oriente fault zone. Apart from these clusters, diffuse
208 seismicity is observed, offshore in the Gulf of Gonâve and along the Septentrional-
209 Oriente and the North Haitian faults in the north of the island.

210

211 **4.2 Focal mechanisms**

212 Using the ISOLA software, 19 focal mechanisms were calculated with the
213 Trans-Haiti network data (Fig. 4, Table 2). We added 7 focal mechanisms
214 calculated by the regional network data from 2015 to 2017 to improve the
215 coverage offshore (Fig. 4, Table 3). Of the 26 focal mechanisms calculated in this
216 study, 14 are shallow (depths < 10 km) with epicenters onland, 8 are located at
217 depths between 10 to 20 km and located along the Enriquillo-Plantain-Garden
218 fault zone, and 4 are located offshore at depths from 20 to 30 km (Fig. 5a). 14 focal
219 mechanisms are compressional, 10 are extensional and 2 are strike-slip (Fig. 5b).
220 The P-axis and T-axis of the 26 centroids are plotted on rose diagrams (Fig. 6). The
221 average P-azimuth is about 15° (NNE-SSW), while the T-axes do not have a very
222 consistent direction although NE-SW is the most dominant.

223

224 **5. Interpretations and Discussion**

225 **5.1 Current deformation**

226 Only two left-lateral strike-slip focal mechanisms are identified on the 26
227 focal mechanisms calculated in this study. They are located along the Enriquillo-
228 Plantain-Garden fault zone (events 24 and 9; Fig. 5a) and associated with an
229 adjacent fault (event 24; Mann et al., 1995) and the fault zone itself near the
230 location of the 2010 earthquake (event 9). The scarcity of this type of event is
231 surprising in this area where a majority of the current deformation is supposed to
232 be strike-slip (Calais et al., 2010; Benford et al., 2012).

233 Of the 26 focal mechanisms calculated in this study, 10 are normal or
234 transtensional (Fig. 5b). On the Southern Peninsula of Haiti, three normal focal
235 mechanisms are aligned along the Enriquillo-Plantain-Garden fault zone (events
236 18, 19 and 10; Fig. 5a). From west to east, they correspond to extensional
237 deformation in L'Asile Basin, the Miragoâne Lake and the Leogâne Quaternary fan
238 delta (Fig. 4)(Mann et al., 1995; Wang et al., 2018), that correspond to extensional
239 step-overs or pull-apart basins along the sinistral strike-slip Enriquillo-Plantain-
240 Garden fault zone. Further east in the Cul-de-Sac basin (Fig. 4), two normal focal
241 mechanisms are also identified on both sides of the Enriquillo Lake (events 15 and
242 13; Fig. 5a) and may be related to normal faults that were mapped previously by
243 Pubellier et al. (2000) in this area. South of the Enriquillo Lake, a normal focal
244 mechanism (event 2; Fig. 5a) can be associated with the collapse of the Sierra de
245 Bahoruco (Fig. 4) along large normal faults (Pubellier et al., 2000). North of the
246 Cul-de-Sac basin, the two other normal focal mechanisms (events 26 and 16; Fig.
247 5a) can be interpreted as extensional fractures on the upper side of folds (extrados
248 faults) or the termination of the subsiding Artibonite valley (Pubellier et al.,
249 2000)(Fig. 4). Offshore in Gulf of Gonâve, two other normal focal mechanisms are
250 identified (events 25 and 22; Fig. 5a). The event 25, at 30 km depth, can be

251 associated with the extensional deformation in half-graben mapped in this area
252 (Leroy et al., 2000). Finally, the event 22 at 9 km depth can be associated with the
253 flat fault ramps identified previously in the Gulf of Gonâve (Corbeau et al., 2016).

254 A majority of the 26 focal mechanisms are thrust-fault related (Fig. 5b). In
255 the Gulf of Gonâve, two thrusts are identified (events 20 and 21; Fig. 5a) and are
256 well correlated with the active compressional deformation mapped in this area by
257 seismic profiles (Corbeau et al., 2016). There are three thrusting events identified
258 on the borders of the Southern Peninsula, one in the north and two in the south
259 (events 17, 12 and 11; Fig. 5a and 5b). In the north, thrusts faults were previously
260 imaged with seismic reflection studies (Bien-Aimé Momplaisir, 1986; Corbeau et
261 al., 2016) and correspond to the thrusting of the Southern Peninsula in the Gulf of
262 Gonâve. In the south, transpressional faults oriented N90° were also imaged by
263 Bien-Aimé Momplaisir (1986) and Mauffret and Leroy (1999) and can be related
264 with the events 12 and 11 of this study. Finally, a cluster of compressional events
265 is identified on the northern side of the Enriquillo Lake (events 1, 3, 4, 5, 6 and 8;
266 Fig. 5b), with a strike-slip component for the event 6. Several studies have
267 previously mapped an active thrust in this area (e.g. Pubellier et al., 2000),
268 interpreted to be the active front of the Trans-Haitian fold and thrust belt. Our
269 results confirm that this thrust is currently active and can produce M3.8
270 earthquakes or possibly larger.

271 Along the Septentrional-Oriente fault zone in the north, two thrust events
272 are identified (events 23 and 7; Fig. 5a). The event 7 (4.5 km depth) is located
273 along the onland segment of the fault zone in Dominican Republic, which is
274 transpressional (Calais et al., 1992b). The recent event of October 7th of 2018 is
275 similar to the event 23 (Fig. 4): both are along the Septentrional-Oriente fault zone

276 and thrust-fault related. The GEOSCOPE Observatory gives a magnitude of 5.9 and
277 a depth of 28 km for the 10/07/2018 event, while we calculate a magnitude of 4.1
278 and a depth of 23 km for the event 23. These depths of 28 and 23 km do not seem
279 to correspond to crustal fault activity. Indeed, receiver functions studies made by
280 Gonzalez et al. (2012) and Corbeau et al. (2017) show that Moho is at about 20 km
281 in the south of Cuba and 23 km in the north of Haiti. This activity under the Moho
282 could be the effect of a slab edge push (van Benthem et al., 2014).

283 The P- and T-axis of the 26 focal mechanisms shown in the rose diagrams
284 (Fig. 6) indicate that the principal compressional stress is trending N-S to NNE-
285 SSW. This orientation is almost perpendicular to the trend of the strike-slip plate
286 boundary in Haiti and is consistent with the results of Calais et al. (1992a) and
287 Mejia and Pulliam (2018) for a large part of the plate boundary. This N-S
288 compressional stress is interpreted to be the result of the collision between the
289 Bahamas platform and Hispaniola. It differs from the generally ENE trend of
290 relative motion in northern Hispaniola determined by GPS measurements (e.g.
291 Benford et al., 2012). Furthermore, the study of van Benthem et al. (2014)
292 proposes that the slab edge push under Hispaniola was the dominant driver of the
293 deformation since 30 Ma, in addition to collision with the Bahamas Platform. In
294 their model, the western edge of the south dipping Puerto Rico slab is moving
295 sideways with the North American plate and produces westward deformation,
296 dominating the collision induced deformation. For the present, both slab edge
297 push mechanism and Bahamas collision reproduce observations (van Benthem et
298 al., 2014). Our results show that the present-day compression, trending N-S to
299 NNE-SSW more clearly reflects the collision with the Bahamas platform.

300

301 **5.2 Seismicity and crustal structure**

302 The year of seismicity recorded in this study is mostly located in the south
303 of Haiti (Fig. 4). This can be explained by a higher rate of tectonic activity in the
304 south of the island, with seismicity associated with the postseismic phase of the
305 Mw 7.0 2010 earthquake (Possee et al., 2019).

306 Figure 7 shows several cross-sections of the seismicity over the study area.
307 The cross-section AA' represents the Gulf of Gonâve area, that is interpreted to be
308 the offshore continuation of the onshore Trans-Haitian Belt, a well-known fold-
309 and-thrust system on Hispaniola (Mann et al., 1995) where N120°E trending north
310 dipping active thrusts have been mapped by Pubellier et al. (2000). Corbeau et al.
311 (2016) show with seismic reflection profiles across the Gulf of Gonâve that there
312 are active folding and thrusts in this area, associated with thrust fault-ramps. The
313 seismicity recorded offshore in the Gulf of Gonâve is distributed over the top 30
314 km of the crust, and may correspond to the thrust fault-ramps inferred from the
315 seismic reflection profiles. Some intermediate-depth earthquakes are also
316 recorded in this area and will be discussed below.

317 The transect CC' (Fig. 7) crosscuts the Cul-de-Sac Basin and the cluster of
318 seismicity near Enriquillo Lake. The cross-section shows that the seismicity is
319 distributed between two thrusts facing each other, the northern side of the
320 Southern Peninsula and the southern side of the Trans-Haitian belt. Between them
321 there are few earthquakes and as shown by Symithe et al. (2016), this diffuse
322 seismicity does not confirm the presence of the Enriquillo-Plantain-Garden fault
323 zone. Several intermediate-depth earthquakes are also recorded in this area and
324 will be discussed in the following section.

325 The transect BB' (Fig. 7) crosscuts the whole of Haiti from the North Haitian
326 fault in the north to the Southern Peninsula. We overlaid the crustal cross-section
327 of Corbeau et al. (2017) made from a receiver function study to indicate the
328 transition between the crustal terranes (in blue, orange and purple) and the
329 mantle (in brown). The majority of the seismicity occurs in the crust, except
330 several events in the southern part of the transect and intermediate-depth
331 earthquakes under the entire cross-section. A cluster of seismicity is present in
332 the north, around the Septentrional-Oriente fault zone. On the enlargement (BB',
333 Fig. 7) the transition between the Southern Peninsula and the Cul-de-Sac basin is
334 marked by segments of the Enriquillo-Plantain-Garden fault zone. The seismicity
335 is distributed at depth in the Southern Peninsula, while it is superficial and sparse
336 in the Cul-de-Sac basin. A cluster of seismicity is identified between the Enriquillo-
337 Plantain-Garden segments, and may be related to the activity following the 2010
338 earthquake. Moreover, a remarkable distribution of events just below the crust-
339 mantle transition is identified (enlargement, BB'; Fig. 7), and seems to be a thrust
340 ramp fault. Such a straight structure was previously proposed by Saint-Fleur et al.
341 (2015).

342

343 **5.3 Intermediate-depth earthquakes under Haiti**

344 On the three cross-sections shown in figure 7, some intermediate-depth
345 earthquakes are identified. These events have depths ranging from ~40 km to 260
346 km and their depths increase southward. Such intermediate-depth seismicity can
347 be related to the presence of a slab or a remnant slab under Haiti. Nevertheless,
348 several authors have previously used the global seismicity and modeled the slab
349 of the North American plate subduction and its edges, and shown that its

350 northwest edge is located in Dominican Republic (Calais et al., 1992a; van
351 Benthem et al., 2013; Symithe et al., 2015; Harris et al., 2018). The deep seismicity
352 reaching ~300 km under Puerto-Rico and Dominican Republic is commonly
353 interpreted as evidence for subducted North American lithosphere. For Calais et
354 al. (1992a), the slab does not exist west of 70°30'W due to the lack of deep
355 seismicity.

356 The new results from the Trans-Haiti network, even over a short time
357 period, indicate that the previous interpretations of the western edge of the North
358 American slab under Hispaniola should potentially be revised. The intermediate-
359 depth earthquakes located in this study are most probably the result of a deep
360 deformation caused by a slab or a remnant slab under Haiti. The lack of seismic
361 stations and permanent network in this area likely made recording of such
362 intermediate-depth seismicity difficult, thus influencing previous interpretations
363 and modeling. A remnant slab is also expected to be less seismically active.
364 According to Calais et al. (1992a), the slab is broken off west of Puerto Rico and is
365 sinking into the mantle under Hispaniola. International Seismological Center
366 global catalogue and our results show that under Haiti, several intermediate-
367 depth earthquakes are present (Fig. 8). Although we do not have enough events to
368 form a clear Benioff zone on the cross-section (DD', Fig. 8), these events are located
369 at expected depths for a subducting slab, or a remnant slab in this region (Symithe
370 et al., 2015).

371

372 **6. Conclusions**

373 We analyze one year of local seismicity in Haiti from the Trans-Haiti
374 temporary network. The new data set shows that the shallow seismicity is well

375 correlated with known tectonic features. The most intense seismicity is located in
376 the south of Haiti, near the 2010 earthquake epicenter and around the Cul-de-Sac
377 basin, with a cluster of compressional earthquakes in the northern side of the
378 Enriquillo Lake. Focal mechanisms are mainly compressional, and the mean
379 compressional P-axis is oriented N-S to NNE-SSW, suggesting that the current
380 deformation is dominated by the collision between the Bahamas platform and
381 Hispaniola. The presence of intermediate-depth earthquakes, ~40-260 km depth,
382 below the Moho suggests the existence of a subducting slab (or possibly a remnant
383 slab) inherited from the frontal subduction of the North American plate under
384 Haiti.

385

386 **ACKNOWLEDGMENTS**

387 We thank SEIS-UK for use of the instruments and their computing facilities. The
388 facilities of SEIS-UK are supported by the Natural Environment Research Council
389 (NERC) under agreement R8/H10/64. This research was partially supported by
390 the European Interreg Caraïbe V program through the PREST project. We are
391 grateful to the team of the OVSM-IPGP for the software provided for the data
392 management. We thank the associate editor Laura Wallace and two anonymous
393 reviewers for helpful comments that improved the manuscript.

REFERENCES CITED

Chapter in a Book/Paper in a Multiauthor Volume

Lomax, A., Virieux, J., Volant, P., and Berge, C., 2000, Probabilistic earthquake location in 3D and layered models: Introduction of a Metropolis-Gibbs method and comparison with linear locations, *in* Thurber, C.H., and Rabinowitz, N., eds., *Advances in Seismic Event Location, Modern Approaches in Geophysics*, Springer, Dordrecht, v. 18, p. 101-134, doi:10.1007/978-94-015-9536-0_5.

Mauffret, A., Leroy, S., 1999, Neogene Intraplate Deformation of the Caribbean Plate at the Beata Ridge, *in* Mann, P., ed., *Caribbean Basins, Sedimentary Basins of the World*, Elsevier, v. 4, p. 627-669, doi:10.1016/S1874-5997(99)80055-0.

Nafe, J.E., and Drake, C.L., 1960, Physical properties of marine sediments, *in* The Sea, Hill M. N., ed., Wiley-Interscience, New-York, v. 3, p. 794-815.

Computer Program

Beyreuther, M., Barsch, R., Krischer, L., Megies, T., Behr, Y. and Wassermann, J., 2010, ObsPy: A Python Toolbox for Seismology, *Seismological Research Letters*, vol. 81, no. 3, p. 530-533, doi: 10.1785/gssrl.81.3.530.

Hanka, W., Saul, J., Weber, B., Becker, J., Harjadi, P., Fauzi, and GITEWS Seismology Group, 2010, Real-time earthquake monitoring for tsunami warning in the Indian Ocean and beyond, *Natural Hazards and Earth System Sciences*, vol. 10, p. 2611-2622, doi:10.5194/nhess-10-2611-2010.

Lee, W. H. K., and Lahr, J. C., 1972, HYP071: A computer program for determining hypocenter, magnitude, and first motion pattern of local earthquakes: U.S. Geological Survey Open-File Report 72-224, 100 p., doi:10.3133/ofr72224.

Database

International Seismological Centre, *On-line Bulletin*, 2016, <http://www.isc.ac.uk>, International Seismological Center, Thatcham, United Kingdom, doi:10.31905/D808B830

Journal Article

Benford, B., DeMets, C., and Calais, E., 2012, GPS estimates of microplate motions, northern Caribbean: Evidence for a Hispaniola microplate and implications for earthquake hazard: *Geophysical Journal International*, v. 191, no. 2, p. 481-490, doi:10.1111/j.1365 246X.2012.05662.x.

van Benthem, S., Govers, R., Spakman, W., and Wortel, R., 2013, Tectonic evolution and mantle structure of the Caribbean: *Journal of Geophysical Research: Solid Earth*, v. 118, no. 6, p. 3019-3036, doi:10.1002/jgrb.50235.

van Benthem, S., Govers, R., and Wortel, R., 2014, What drives microplate motion and deformation in the northeastern Caribbean plate boundary region? : *Tectonics*, v. 33, no. 5, p. 850-873, doi:10.1002/2013TC003402.

Burke, K., 1988, Tectonic evolution of the Caribbean: *Annual Review of Earth and Planetary Sciences*, v. 16, p. 201-230, doi:10.1146/annurev.earth.16.050188.001221.

Calais, E., and Mercier de Lépinay, B., 1991, From transtension to transpression along the northern Caribbean plate boundary off Cuba: Implications for the recent motion of the Caribbean plate: *Tectonophysics*, v. 186, no. 3-4, p. 329-350, doi:10.1016/0040-1951(91)90367-2.

Calais, E., Béthoux, N., and Mercier de Lépinay, B., 1992a, From transcurrent faulting to frontal subduction: A seismotectonic study of the northern Caribbean plate boundary from Cuba to Puerto Rico: *Tectonics*, v. 11, no. 1, p. 114-123, doi:10.1029/91TC02364.

Calais, E., Mercier de Lépinay, B., Saint-Marc, P., Butterlin, J., and Schaaf, A., 1992b, La Limite de plaques décrochante nord caraïbe en Hispaniola ; evolution paleogeographique et structurale cenozoïque: *Bulletin de la Société Géologique de France*, v. 163, no. 3, p. 309-324.

Calais, E., Mazabraud, Y., Mercier de Lépinay, B., Mann, P., Mattioli, G., and Jansma, P., 2002, Strain partitioning and fault slip rates in the northeastern Caribbean from GPS measurements: *Geophysical Research Letters*, v. 29, no. 18, p. 1856, doi:10.1029/2002GL015397.

Calais, E., Freed, A., Mattioli, G., Amelung, F., Jónsson, S., Jansma, P., Hong, S.-H., Dixon, T., Prépetit, C., and Momplaisir, R., 2010, Transpressional rupture of an unmapped fault during the 2010 Haiti earthquake: *Nature Geosciences*, v. 3, no. 11, p. 794-799, doi:10.1038/ngeo992.

Corbeau, J., Rolandone, F., Leroy, S., Meyer, B., Mercier de Lépinay, B., Ellouz-Zimmermann, N., and Momplaisir, R., 2016, How transpressive is the Northern Caribbean plate boundary? : *Tectonics*, v. 35, no. 4, p. 1032-1046, doi:10.1002/2015TC003996.

Corbeau, J., Rolandone, F., Leroy, S., et al., 2017, Crustal structure of western Hispaniola (Haiti) from a teleseismic receiver function study: *Tectonophysics*, v. 709, p. 9-19, doi:10.1016/j.tecto.2017.04.029.

Cruz-Orosa, I., Sàbat, F., Ramos, E., Rivero, L., Vázquez-Taset, Y.M., 2012. Structural evolution of the La Trocha fault zone: oblique collision and strike-slip basins in the Cuban Orogen: *Tectonics*, v. 31, no. 5, doi:10.1029/2011TC003045.

Douilly, R., et al., 2013, Crustal structure and fault geometry of the 2010 Haiti earthquake from temporary seismometer deployments: *Bulletin of the Seismological Society of America*, v. 103, no. 4, p. 2305-2325, doi:10.1785/0120120303.

Escuder Viruete, J., Contreras, F., Stein, G., Urien, P., Joubert, M., Ullrich, T.D., Mortensen, J., Perez Estaun, A., 2006. Transpression and strike-slip partitioning in the Caribbean island arc: fabric development, kinematics and Ar-Ar ages of syntectonic emplacement of the Loma de Cabrera batholith, Dominican Republic: *Journal of Structural Geology*, v. 28, p. 1496-1519, doi:10.1016/j.jsg.2006.04.003.

Bruña, J. G., Carbó-Gorosabel, A., Estrada, P. L., Muñoz-Martín, A., Ten Brink, U. S., Ballesteros, M. G., Druet, M., and Pazos, A., 2014, Morphostructure at the junction between the Beata ridge and the Greater Antilles island arc (offshore Hispaniola southern slope): *Tectonophysics*, v. 618, p. 138-163, doi:10.1016/j.tecto.2014.02.001.

González, O. L., Moreno, B., Romanelli, F., and Panza, G. F., 2012, Lithospheric structure below seismic stations in Cuba from the joint inversion of Rayleigh surface waves dispersion and receiver functions: *Geophysical Journal International*, v. 189, no. 2, p. 1047-1059, doi:10.1111/j.1365-246X.2012.05410.x.

Graves, R. W., and Pitarka, A., 2010, Broadband ground-motion simulation using a hybrid approach: *Bulletin of the Seismological Society of America*, v. 100, no. 5A, p. 2095-2123, doi:10.1785/0120100057.

Harris, C. W., Miller, M. S., and Porritt, R. W., 2018, Tomographic Imaging of Slab Segmentation and Deformation in the Greater Antilles: *Geochemistry, Geophysics, Geosystems*, v. 19, no. 8, p. 2292-2307, doi:10.1029/2018GC007603.

Iturralde-Vinent, M.A., 2006, Meso-Cenozoic Caribbean paleogeography: implications for the historical biogeography of the region: *International Geology Review*, v. 48, no. 9, p. 791-827, doi:10.2747/0020-6814.48.9.791.

Křížová, D., Zahradník, J., and Kiratzi, A., 2013, Resolvability of isotropic component in regional seismic moment tensor inversion: *Bulletin of the Seismological Society of America*, v. 103, no. 4, p. 2460-2473, doi:10.1785/0120120097.

Leroy, S., Mercier de Lépinay, B., Mauffret, A., and Pubellier, M., 1996, Structural and tectonic evolution of the eastern Cayman Trough (Caribbean Sea) from seismic reflection data: *AAPG Bulletin*, v. 80, no. 2, p. 222-247.

Leroy, S., Mauffret, A., Patriat, P., and Mercier de Lépinay, B., 2000, An alternative interpretation of the Cayman trough evolution from a reidentification of magnetic anomalies: *Geophysical Journal International*, v. 141, no. 3, p. 539-557, doi:10.1046/j.1365-246x.2000.00059.x.

Leroy, S., Ellouz-Zimmermann, N., Corbeau, J., et al., 2015, Segmentation and kinematics of the North America-Caribbean plate boundary offshore Hispaniola: *Terra Nova*, v. 27, no. 6, p. 467-478, doi:10.1111/ter.12181.

Mann, P., Taylor, F., Edwards, R. L., and Ku, T.-L., 1995, Actively evolving microplate formation by oblique collision and sideways motion along strike-slip faults: An example from the northeastern Caribbean plate margin: *Tectonophysics*, v. 246, no. 1, p. 1-69, doi:10.1016/0040-1951(94)00268-E.

McCann, W. R., and Sykes, L. R., 1984, Subduction of aseismic ridges beneath the Caribbean plate: Implications for the tectonics and seismic potential of the northeastern Caribbean: *Journal of Geophysical Research: Solid Earth*, v. 89, no. B6, p. 4493-4519, doi:10.1029/JB089iB06p04493.

Mejia, H., and Pulliam, J., 2018, P-and T-Axis Probabilities (PaTaPs): Characterizing Regional Stress Patterns with Probability Density Functions of Fault-Plane Uncertainties: *Seismological Research Letters*, doi:10.1785/0220180112.

Mercier de Lépinay, B., et al., 2011, The 2010 Haiti earthquake: A complex fault pattern constrained by seismologic and tectonic observations: *Geophysical Research Letters*, v. 38, no. L22305, doi:10.1029/2011GL049799.

Pindell, J., Kennan, L., Draper, G., Maresch, W. V., and Stanek, K. P., 2006, Foundations of Gulf of Mexico and Caribbean evolution: eight controversies resolved: *Geologica Acta: an international earth science journal*, v. 4, no. 1, p. 303-341.

Possee, D., Keir, D., Harmon, N., Rychert, C., Rolandone, F., Leroy, S., Corbeau, J., Stuart, G., Calais, E., Illsley-Kemp, F., Boisson, D., Momplaisir, R., and Prépetit, C., 2019, The Tectonics and Active Faulting of Haiti from Seismicity and Tomography: *Tectonics*, doi:10.1029/2018TC005364.

Pubellier, M., Mauffret, A., Leroy, S., Vila, J. M., and Amilcar, H., 2000, Plate boundary readjustment in oblique convergence: Example of the neogene of Hispaniola, Greater Antilles: *Tectonics*, v. 19, no. 4, p. 630-648, doi:10.1029/2000TC900007.

Saint Fleur, N., Feuillet, N., Grandin, R., Jacques, E., Weil-Accardo, J., and Klinger, Y., 2015, Seismotectonics of southern Haiti: a new faulting model for the 12 January 2010 M7 earthquake: *Geophysical Research Letters*, v. 42, no. 23, p. 10,273-10,281, doi:10.1002/2015GL065505.

Sokos, E. N., and Zahradnik, J., 2008, ISOLA a Fortran code and a Matlab GUI to perform multiple-point source inversion of seismic data: *Computers & Geosciences*, v. 34, no. 8, p. 967-977, doi:10.1016/j.cageo.2007.07.005.

Sokos, E. N., and Zahradník, J., 2013, Evaluating centroid-moment-tensor uncertainty in the new version of ISOLA software: *Seismological Research Letters*, v. 84, no. 4, p. 656-665, doi:10.1785/0220130002.

Symithe, S., Calais, E., Chabalier, J. B., Robertson, R., and Higgins, M., 2015, Current block motions and strain accumulation on active faults in the Caribbean: *Journal of Geophysical Research: Solid Earth*, v. 120, p. 3748-3774, doi:10.1002/2014JB011779.

Symithe, S., and Calais, E., 2016, Present-day shortening in Southern Haiti from GPS measurements

and implications for seismic hazard: *Tectonophysics*, v. 679, p. 117–124, doi:10.1016/j.tecto.2016.04.034.

Wang, J., Mann, P., and Stewart, R. R., 2018, Late Holocene structural style and seismicity of highly transpressional faults in southern Haiti, *Tectonics*, doi:10.1029/2017TC004920.

Zahradník, J., and Custódio, S., 2012, Moment tensor resolvability: Application to southwest Iberia: *Bulletin of the Seismological Society of America*, v. 102, no. 3, p. 1235-1254, doi:10.1785/0120110216.

Thesis

Bien-Aimé Momplaisir, R., 1986. Contribution à l'étude géologique de la partie orientale du Massif de la Hotte (Presqu'île du Sud d'Haïti): Synthèse structurale des marges de la presqu'île à partir de données sismiques [Ph.D. thesis]: Paris, Université Pierre et Marie Curie, 210 p.

Boisson, D., 1987, Etude géologique du massif du nord d'Haïti (Hispaniola-grandes Antilles), [Ph.D. thesis]: Paris, Université Pierre et Marie Curie, 215 p.

Dorel, J., 1978, Sismicité et structure de l'arc des Petites Antilles et du bassin Atlantique [Ph.D. thesis]: Paris, Université Pierre et Marie Curie, 326 p.

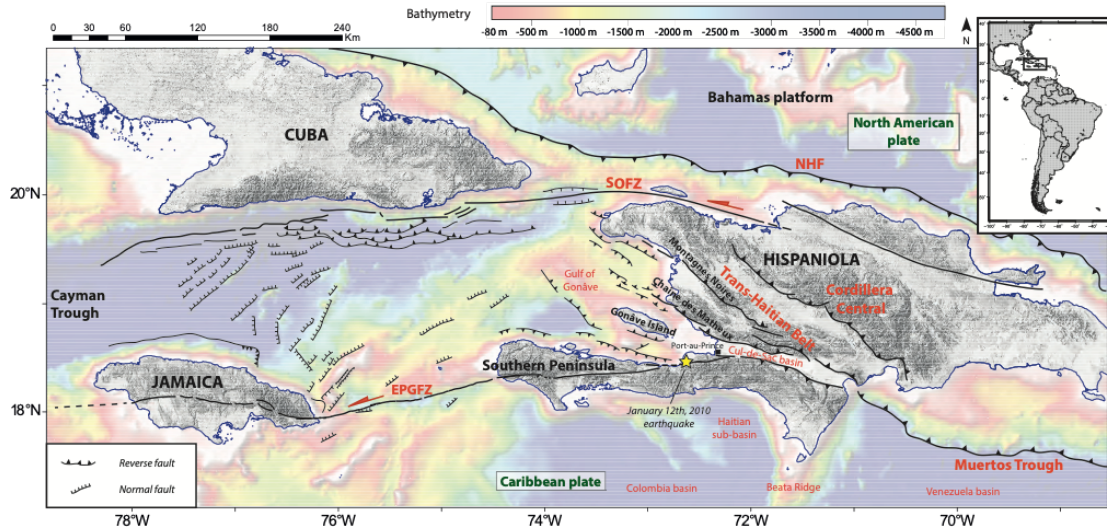


Figure 1: Tectonic map of the northern Caribbean plate boundary in the Hispaniola region. NHF: North Haitian Fault; SOFZ: Septentrional-Oriente Fault Zone; EPGFZ: Enriquillo-Plantain-Garden Fault Zone. Faults are from previous studies (Calais and Mercier de Lepinay, 1991; Mann et al., 1995; Leroy et al., 1996, 2015; Granja-Bruña et al., 2014).

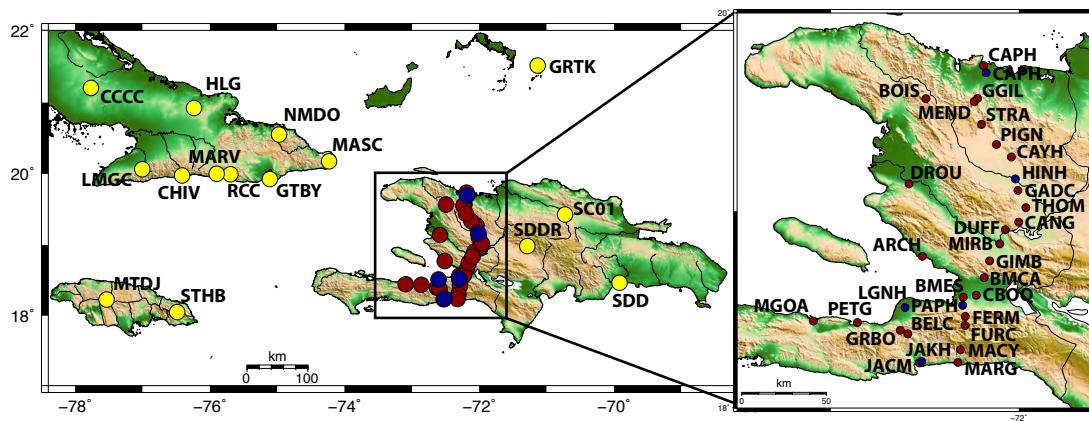
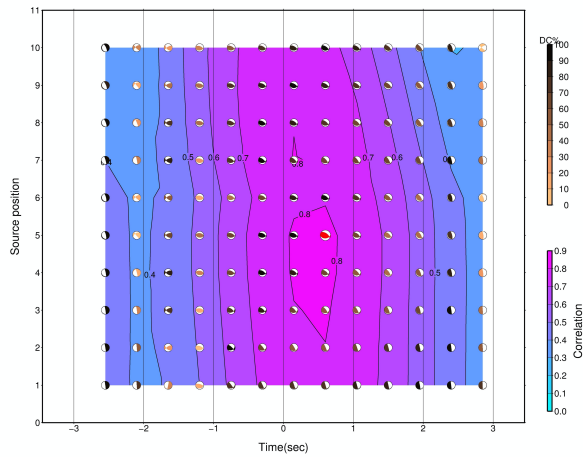


Figure 2: Map of the stations used in this study. The red dots are the temporary seismic stations of the Trans-Haiti network deployed from 2013 to 2014. The blue dots are the Haitian permanent stations of the Canadian network. The yellow dots are permanent stations from Cuba, Jamaica, Bahamas and Dominican Republic.

(A)



(B)

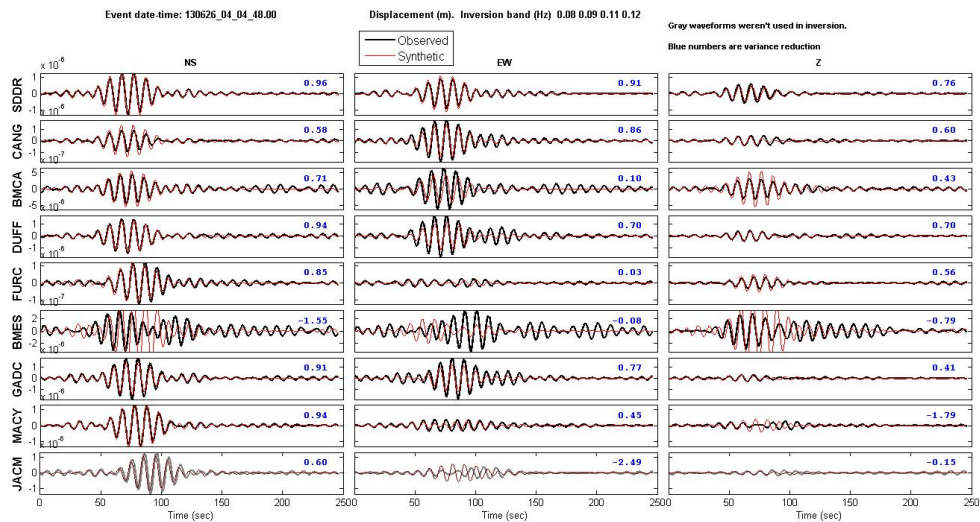


Figure 3: (A) Representation of a vertical grid search for the 2013/06/26 04:04:48 UTC earthquake. The vertical grid search is done in 10 trial positions around the hypocenter (starting depth is 1 km and vertical step is 1 km) and around the origin time (the range is +/- 3 s with a step of 0.45 s). The best-fitting solution is represented by the red beach ball (largest correlation). The color of the other beach balls represents the double-couple percentage (DC%). This is a representative example for the clarity of the grid. The steps used in this study are mentioned in the text part 3.3. (B) Example of the synthetic waveforms (in red)

versus the observed waveform (in black) for the 2013/06/26 04:04:48 UTC earthquake. The variance reduction values are indicated in blue for each component.




Event #	Origine time yyyymmdd hh:mm:ss.ss	Lat Lon	Depth	Mw	Strike Dip Rake NP1	Strike Dip Rake NP2	Mom Ten	DC %	VR %	NC	SNR	K°	CN
This study	20140528 21:15:01.00	18.22 -67.97	105,0	5.8	34 23 56	250 71 103		98.6	52	18	44	5.4	4.5
CGMT	20140528 21:15:07.90	18.40 -68.36	89,0	5.8	29 30 44	259 69 113							
USGS	20140528 21:15:06.00	18.05 -68.35	100,5	5.8	36 31 48	263 68 112							
This study	20131128 19:28:48.00	18.98 -71.81	0,5	3									
TNT shot	20131128	18.98 -71.78	0,1										

Table 1: Comparison of the hypocenters and the fault-plane solutions for the 2014/05/28 M5.8 event between our study and the GCMT and USGS catalogs; comparison between the position of a TNT shot and its localization with our data set. DC%: double-couple percentage; VR%: variance reduction percentage; NC: number of components used; SNR: signal to noise ratio; K°: mean Kagan angle; CN: condition number.

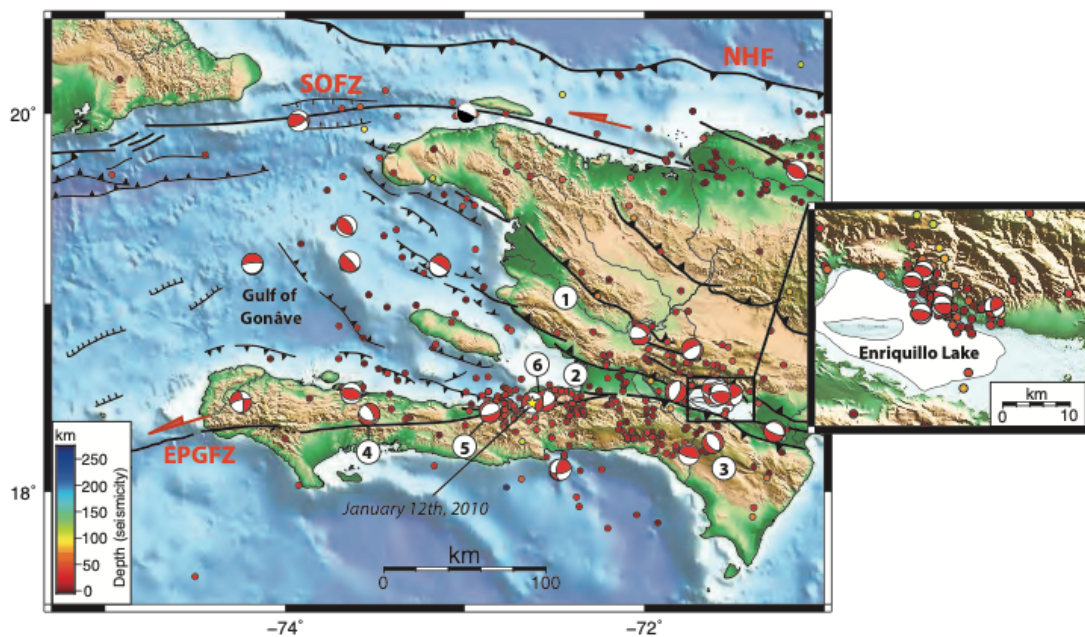


Figure 4: Local seismicity in Haiti from June 2013 to June 2014 and focal mechanisms calculated in this study. The black focal mechanism in the north of Haiti is from Geoscope and related to the 10/07/2018 event. NHF: North Haitian Fault; SOFZ: Septentrional-Oriente Fault Zone; EPGFZ: Enriquillo-Plantain-Garden Fault Zone. Enlargement: Enriquillo Lake. Numbers are for: 1- Artibonite Valley; 2- Cul-de-Sac Basin; 3- Sierra de Bahoruco; 4- L'Asile Basin; 5- Miragoâne Lake and 6- Leogâne fan delta.

Event #	Origine time yyyymmdd hh:mm:ss.ss	Lat Lon hypocenter	Depth hypocenter	Lat Lon centroid	Depth centroid	Mv	Mw	Strike Dip Rake NP1	Strike Dip Rake NP2	Mom Ten	DC %	VR %	NC	SNR	K°	CN
1	20130612 05:29:05.00	18.51 -71.55	3,0	18.56 -71.60	2,0	3.1	3.5	293 50 110	83 44 67		74.5	52	30	4	3.5	2.3
2	20130621 20:09:46.00	18.28 -71.63	2,1	18.26 -71.61	7,0	3.6	3.8	330 39 -82	140 52 -96		75.7	51	9	2	8	6.4
3	20130625 22:34:04.00	18.51 -71.53	2,9	18.50 -71.60	2,2	3	3.8	76 28 67	281 64 102		92.5	68	21	15	3.9	3.1
4	20130626 04:04:48.00	18.51 -71.54	2,5	18.54 -71.62	2,5	3.2	3.8	94 40 85	281 50 94		97.8	77	24	13	3	2.6
5	20130630 16:05:33.00	18.55 -71.60	-0,6	18.53 -71.57	2,0	3.1	3	99 10 79	290 80 92		83	36	9	6	6.4	4
6	20130712 10:22:04.00	18.51 -71.51	4,2	18.51 -71.51	3,0	3.3	3.4	69 64 149	174 63 30		38.7	35	12	7	6.9	3.7
7	20130718 01:54:39.00	19.74 -71.20	-1,8	19.69 -71.15	4,5	3.3	3.6	308 55 98	114 36 78		64.4	48	9	4	11.7	5.4
8	20130829 17:02:49.00	18.51 -71.58	-0,7	18.51 -71.58	2,5	2.7	3.1	138 32 137	266 69 66		86.3	45	9	16	6.5	1.6
9	20130922 02:25:25.00	18.47 -72.62	14,4	18.47 -72.62	13,0	2.7	3.1	153 87 170	243 80 3		63.4	51	15	2	16.3	9.2
10	20131012 17:59:15.00	18.48 -72.57	15,2	18.48 -72.55	10,7	2.8	3.5	76 50 -28	185 69 -137		94.7	42	15	5	5.6	3.1
11	20131221 23:07:20.00	18.14 -72.44	13,4	18.12 -72.47	26,8	2.8	4.4	64 70 132	175 46 29		35.6	82	12	32	5.3	4.2
12	20131222 04:48:49.00	18.13 -72.45	14,3	18.11 -72.46	26,6	2.7	3.6	190 57 36	78 61 141		60.3	45	12	3	4.6	4.5
13	20140123 03:16:16.00	18.34 -71.33	7,5	18.32 -71.27	12,5	3.2	3.6	296 19 -88	113 71 -91		66.7	39	12	3	3.7	3.3
14	20140201 11:29:26.00	18.21 -71.67	5,0	18.19 -71.75	9,5	3.3	3.5	105 70 95	271 20 76		81.2	37	9	5	7	4.7
15	20140212 23:20:55.0	18.53 -71.82	12,5	18.53 -71.82	18,0	3.8	3.7	25 62 -83	191 29 -102		98.2	43	12	12	5.3	3.5
16	20140313 20:34:53.00	18.68 -71.65	11,5	18.75 -71.73	3,5	2.9	2.9	24 22 -126	243 73 -77		90.7	53	9	2	4.4	2
17	20140322 01:11:40.32	18.52 -73.67	12,0	18.52 -73.63	7,0	3.9	4.2	285 53 96	95 38 82		74.3	49	27	2	3.6	3.8
18	20140510 18:27:22.00	18.38 -73.56	9,6	18.41 -73.53	17,6	3.3	3.9	334 63 -60	102 40 -135		47.7	60	12	3	12.5	5.7
19	20140526 09:18:11.00	18.42 -72.82	37,9	18.42 -72.86	18,0	2.5	3.9	226 27 -116	75 66 -78		36.9	62	12	8	5.5	3.9

Table 2: Focal mechanisms calculated in this study with the Trans-Haiti network dataset. See caption of Table 1 for the abbreviations.

Event #	Origine time yyyymmdd hh:mm:ss.ss	Lat Lon hypocenter	Depth hypocenter	Lat Lon centroid	Depth centroid	Mw	Strike Dip Rake NP1	Strike Dip Rake NP2	Mom Ten	DC %	VR %	NC	SNR	K°	CN
20	20150717 12:23:09.10	19.29 -73.69	33,0	19.21 -73.63	29,0	4.4	107 12 61	317 80 96		97.3	53	17	16	3.1	2.1
21	20151231 02:20:43.00	19.43 -73.63	10,0	19.40 -73.66	13,0	4.7	128 35 77	324 56 99		52.9	63	26	18	3.5	2.2
22	20160106 17:55:57.30	19.19 -73.08	23,0	19.19 -73.14	9,0	4.2	302 82 -86	93 9 -118		98.1	61	13	7	4.4	1.9
23	20160328 13:57:32.50	19.82 -73.86	10,0	19.96 -73.92	23,0	4.1	59 64 55	297 43 139		79.2	68	19	8	6.3	3.2
24	20161112 06:00:50.00	18.45 -74.24	31,0	18.47 -74.24	18,0	4	352 72 -161	256 72 -19		90	64	18	10	4.8	2.1
25	20170620 19:01:18.60	19.20 -74.18	5,0	19.20 -74.18	30,0	4.5	265 79 -85	60 12 -115		73.9	30	18	30	3.5	2.4
26	20170902 20:14:08.00	18.94 -72.05	15,7	18.83 -72.02	9,0	4.4	311 49 -45	74 58 -129		63.6	82	15	12	5.3	2.3

Table 3: Focal mechanisms calculated in this study with the Cuban network. See caption of Table 1 for the abbreviations.

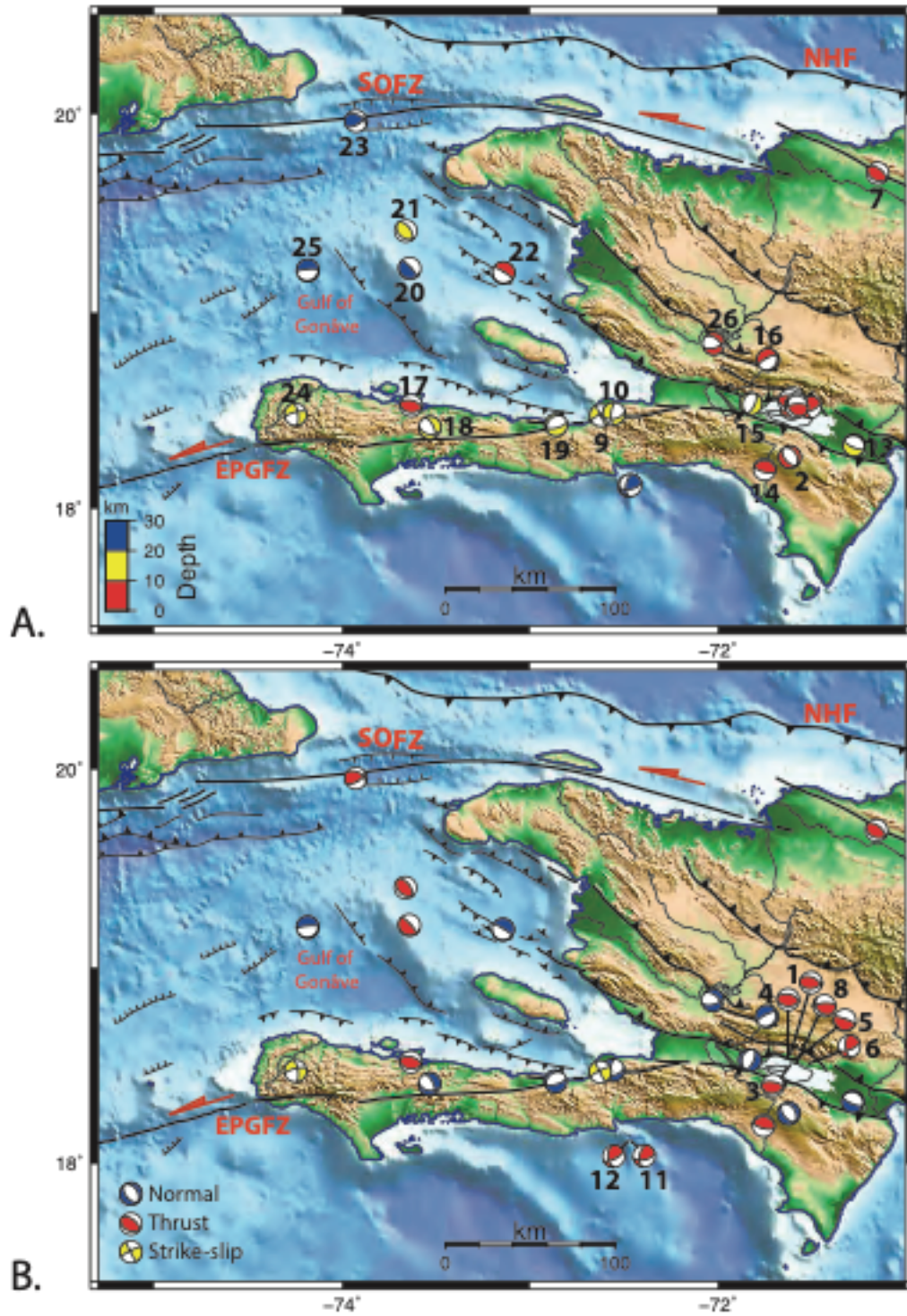


Figure 5: A. Distribution of the focal mechanisms as a function of depth; B. Distribution of the focal mechanisms as a function of slip type.

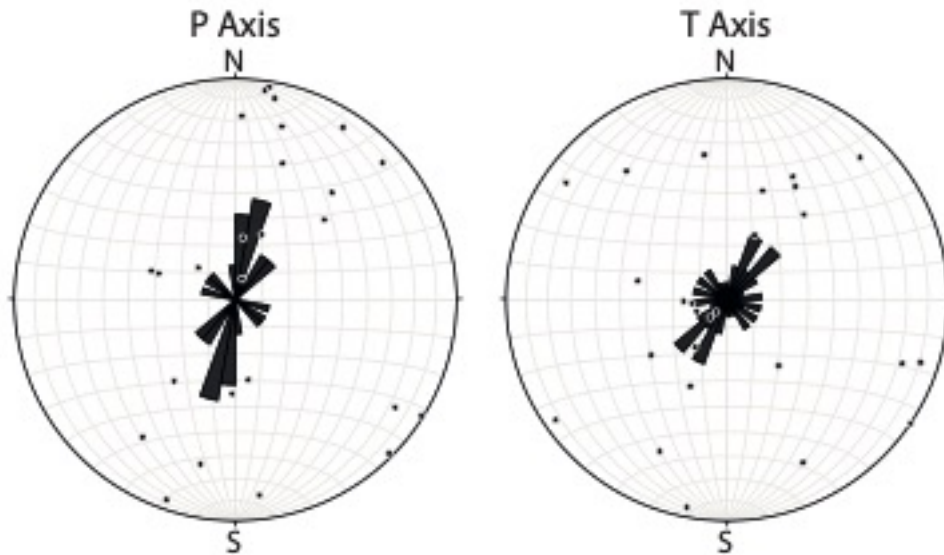


Figure 6: Rose diagrams for the P- (left) and T-axis (right) of the 26 focal mechanisms calculated in this study. The P- and T-axis indicate that the principal compressional stress is trending N-S to NNE-SSW.

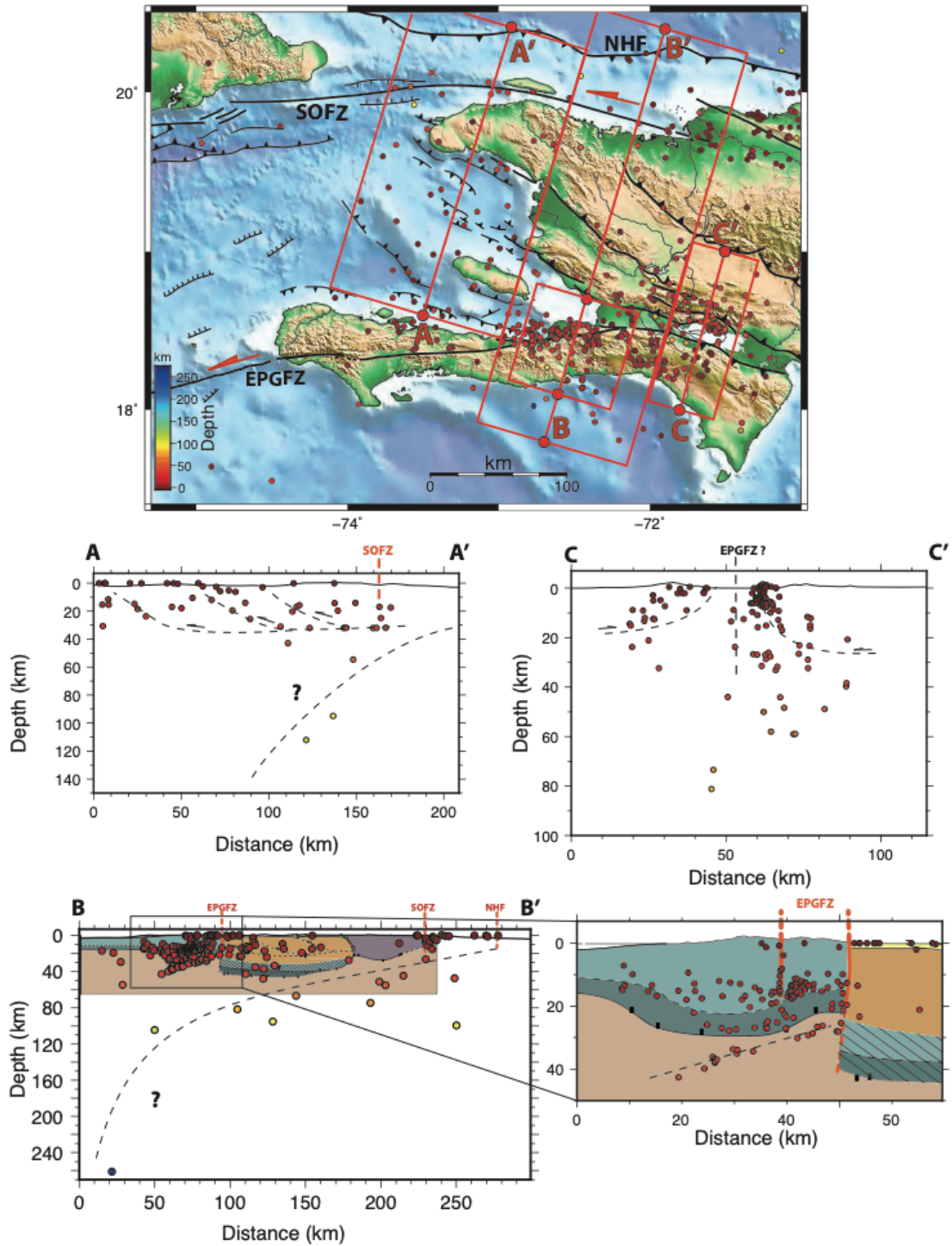


Figure 7: Cross-sections of seismicity. NHF: North Haitian Fault; SOFZ: Septentrional-Oriente Fault Zone; EPGFZ: Enriquillo-Plantain-Garden Fault Zone. On the C-C cross-section and its enlargement, we overlaid the crustal cross-section of Corbeau et al. (2017) made from a receiver function study. The crustal terranes are in blue, orange and purple. The brown part represents the mantle.

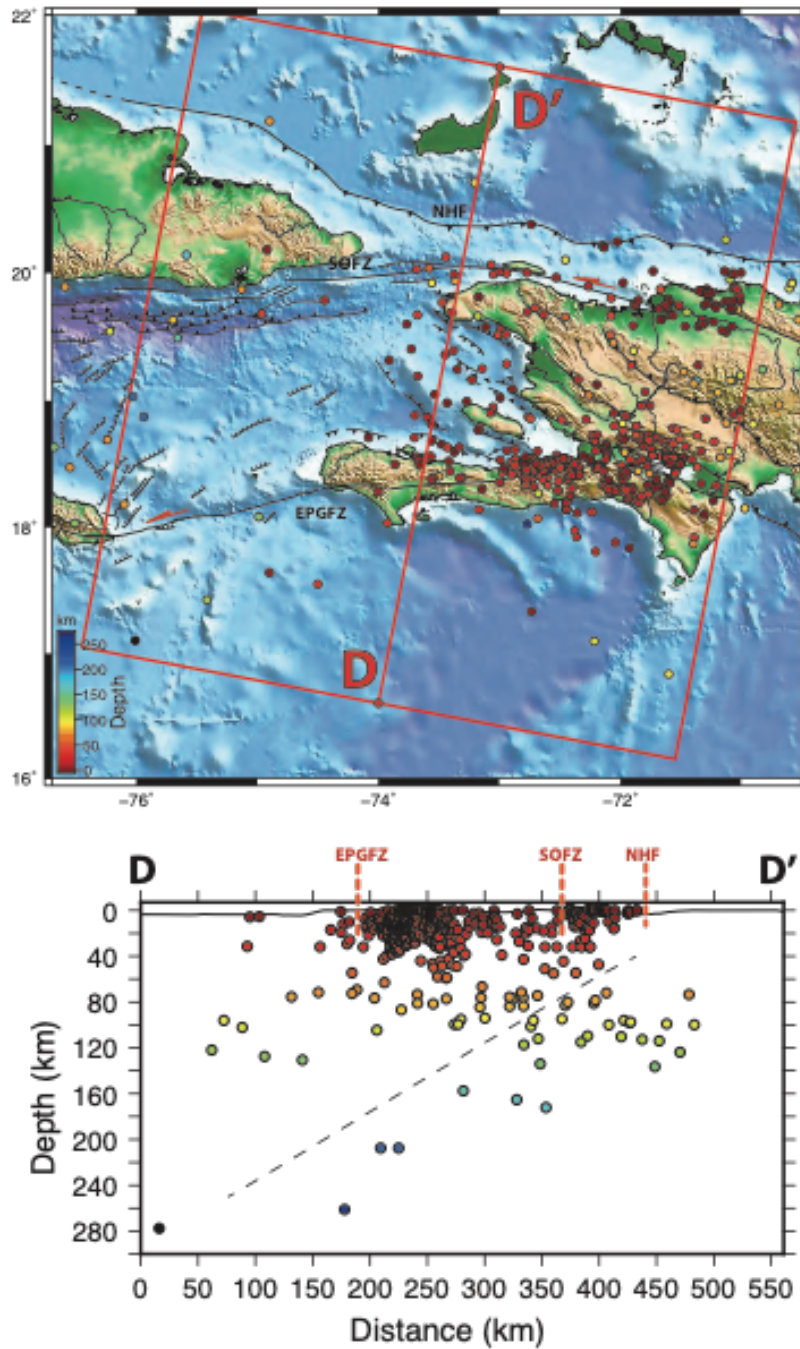


Figure 8: Local seismicity of this study overlaid on the International Seismological Center global reviewed catalog (seismicity from 1950 to 2005, hypocenters > 70 km depth) and the associated cross-section. NHF: North Haitian Fault; SOFZ: Septentrional-Oriente Fault Zone; EPGFZ: Enriquillo-Plantain-Garden Fault Zone.